Structural Relaxation is a Scale-Free Process

Anaël Lemaître*
Université Paris-Est, Laboratoire Navier (UMR 8205), CNRS, ENPC, IFSTTAR, 2 allée Képler, F-77420 Marne-la-Valle, France
(Received 18 June 2014; published 11 December 2014)

We show that in deeply supercooled liquids, structural relaxation proceeds via the accumulation of Eshelby events, i.e. local rearrangements that create long-ranged and anisotropic stresses in the surrounding medium. Such events must be characterized using tensorial observables and we construct an analytical framework to probe their correlations using local stress data. By analyzing numerical simulations, we then demonstrate that events are power-law correlated in space, with a time-dependent amplitude which peaks at the alpha relaxation time τ_α. This effect, which becomes stronger near the glass transition, results from the increasingly important role of local stress fluctuations in facilitating relaxation events. Our finding precludes the existence of any length scale beyond which the relaxation process decorrelates.

DOI: 10.1103/PhysRevLett.113.245702 PACS numbers: 64.70.Q-, 05.20.Jj, 61.43.Fs, 62.20.D-

For two decades, the main approach to structural relaxation has focused on "mobility heterogeneities," i.e., regions of space where atoms undergo large displacements over some time window [1–10]. These heterogeneities are probed using scalar moments of the displacement field, which systematically decorrelate exponentially in space. It has thus become customary to expect that the relaxation process also does. But the precise relation between these observables and the actual relaxation mechanisms has never been clarified. It hence remains necessary to first identify the elementary processes governing relaxation before constructing tailored observables that can probe and correlate their occurrence in distant regions of space. We here follow this route by elaborating upon the idea that highly viscous liquids are "solids which flow" [11–14], a notion which motivates various attempts to relate relaxation to stress or elastic properties [15–24].

In deep supercooling, relaxation proceeds via a series of activated hops between inherent structures (or ISs), i.e., local minima of the potential energy surface [25–27]. Each IS is by definition a mechanically stable configuration, that is, an elastic solid, and the ensemble of ISs explored by an equilibrated liquid constitutes the glassy state where it is trapped if suddenly quenched at low temperature. Accordingly, the relaxation of a supercooled liquid results from the accumulation of activated transitions between configurations of the corresponding (underlying) glass. Now, elasticity theory [28,29] asserts that any localized irreversible event occurring in a solid creates so-called Eshelby stresses, which have no characteristic length scale (decay as power laws) and are anisotropic [12,30]. These fields are clearly documented in sheared glasses [31–34], and evidence was found recently for their presence in sheared liquids [35].

Here, using a 2D numerical model of a quiescent supercooled liquid, we show that relaxation results from the accumulation of Eshelby events, i.e., local rearrangements which give rise to elastic strains in the embedding medium. We propose to characterize events by their *elastic dipoles*, a tensorial quantity, which accounts for the local shape change in a rearrangement, and fully determines the long-ranged Eshelby stress field. We construct an analytical framework to relate the density of dipoles accumulated over a given time window, to the increment of local IS stress. By systematically analyzing the correlation matrix of stress increments we then demonstrate that events are power-law correlated in space, with a time-dependent amplitude.

Simulations are performed using the same 2D binary Lennard-Jones (LJ) model as in [32–36]. All quantities are given in reduced LJ units. The simulation cell is square, of size $L \times L$, and biperiodic, with Bravais axes x and y. All data points are obtained in equilibrium for each temperature T; ISs are computed at regular times.

Coarse-grained stress fields $\sigma_{\alpha\beta}(\underline{r};t)$ are computed in ISs [36,37]. In two dimensions, stress has three independent components, which we decompose as pressure $\sigma_1 \equiv -\frac{1}{2}(\sigma_{xx}+\sigma_{yy})$, normal $\sigma_2 \equiv \frac{1}{2}(\sigma_{xx}-\sigma_{yy})$, and shear stress $\sigma_3 \equiv \sigma_{xy}$. These fields are plotted on Fig. 1, for an $L = 80$ system equilibrated at $T = 0.26$, a temperature at which $\tau_\alpha \approx 10^4$ [36]. σ_1 is isotropic, but strikingly both σ_2 and σ_3 are anisotropic. This is quite unexpected but

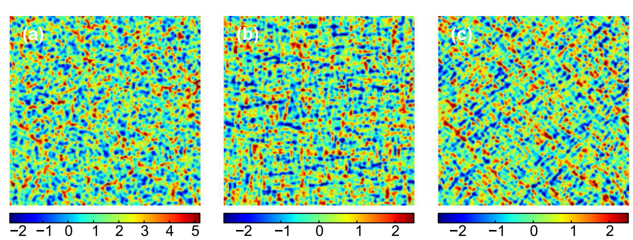

FIG. 1 (color online). In an IS of an $L = 80$ system equilibrated at $T = 0.26$. (a) Pressure, σ_1 (b) $\sigma_2 \equiv \frac{1}{2}(\sigma_{xx}-\sigma_{yy})$, and (c) $\sigma_3 = \sigma_{xy}$.

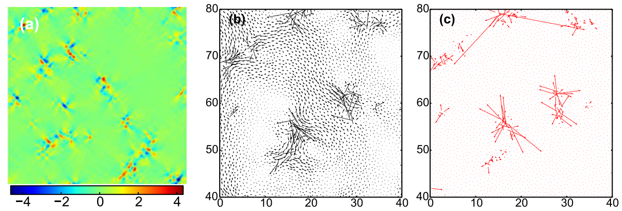

FIG. 2 (color online). For $L = 80$, $T = 0.26$, $t = 100$. (a) $\delta\sigma_3(\underline{r}; t_0, t_0 + t)$, (b),(c) the associated displacement and force fields, respectively, in the upper-left quarter of the cell (see x, y coordinates).

perfectly consistent with the structural isotropy of our system, which requires pressure to be isotropic, but only demands σ_2 (which is the shear stress in a frame rotated by $\pi/4$ from the x, y axes) to be statistically equivalent to σ_3 up to a $\pi/4$ rotation. These anisotropies will be explained only at the end of our discussion.

From the same system, we pick two ISs separated by a time interval $t = 100 \ll \tau_\alpha \approx 10^4$ and image on Fig. 2 their local differences. On the map [Fig. 2(a)] of the local shear stress increment $\delta\sigma_3(\underline{r}; t_0, t_0+t) = \sigma_3(\underline{r}; t_0+t) - \sigma_3(\underline{r}; t_0)$ relaxation events show up as conspicuous color spots, corresponding to large and random stress changes. In the displacement field [Fig. 2(b)] $\{\underline{u}_i\}$, with i the particle index (only the upper left quarter of the system is shown), jumbles of large arrows reveal a few localized events connected by swirls of small, smoothly varying, displacements. Since the distance between events is rather large—ten to twenty particles—these swirls are quite long ranged and, hence, suggest that the amorphous matrix is responding elastically.

In the linear approximation about the $t_0 + t$ IS, the displacement field $\{\underline{u}_i\}$ can be viewed as the elastic response to the forces $\underline{f}_i = \sum_j \underline{\underline{H}}_{ij} \cdot \underline{u}_j$, with $\underline{\underline{H}}_{ij}$ the Hessian [38]. As shown on Fig. 2(c), $\{\underline{f}_i\}$ is strongly localized on relaxation centers: the broad areas where it vanishes hence respond linear elastically. This now confirms that the swirls of $\{\underline{u}_i\}$ are due to elastic strains, and, consequently, that events are of Eshelby type [28]: each one corresponds to a change of inherent configuration for a small group of atoms embedded in the amorphous structure; when it occurs, the core atoms must find mechanical equilibrium with the embedding medium: that is why the latter must elastically deform.

It appears from the above construction that the strains generated by events are equivalent to the elastic response to a localized force field. Now, the perturbations created in an amorphous structure by pointlike forces match at long range the prediction of continuum elasticity [39]. And elasticity theory asserts [29,30] that the incremental stress generated by a group of forces applied at points $\underline{r}_i$ localized around the origin of an isotropic elastic continuum does not depend, in the far field, on all microscopic details of these forces, but on the associated "dipole" $\sum_i \underline{f}_i \underline{r}_i$. We thus characterize an event occurring around $\underline{r}_e$ by the dipole density $\underline{\underline{\rho}}^e = -\delta(\underline{r} - \underline{r}_e)\sum_i \underline{f}_i \underline{r}_i$: with this sign convention, the stress "released" is $\frac{1}{L^2}\int \underline{\underline{\rho}}^e$ [30].

In [36], we evaluate the total stress change $\delta\underline{\underline{\sigma}}$ due to an event occurring at the origin of a 2D isotropic elastic medium. Our calculation is fully tensorial and yields, in Fourier space (with ^ marking the Fourier transforms), a relation of the form $\delta\hat{\underline{\underline{\sigma}}} = \hat{E} \cdot \hat{\underline{\underline{\rho}}}^e$ with $\hat{E}$ a fourth order Green tensor. Using the vector notation $\underline{\sigma} \equiv [\sigma_1, \sigma_2, \sigma_3]$ for symmetric tensors, $\hat{E}$ writes as the matrix

$$\begin{pmatrix} A_E & \alpha_E\cos(2\phi) & \alpha_E\sin(2\phi) \\ \beta_E\cos(2\phi) & B_E + \gamma_E\cos(4\phi) & \gamma_E\sin(4\phi) \\ \beta_E\sin(2\phi) & \gamma_E\sin(4\phi) & B_E - \gamma_E\cos(4\phi) \end{pmatrix}, \tag{1}$$

with ϕ the azimuth of the wave vector $\underline{k}$. $A_E, B_E, \alpha_E, \beta_E, \gamma_E$ are > 0 constants. Each element of $\hat{E}(\underline{k})$ relates a component of the source density $\hat{\rho}^e_k$ to one of the incremental stress $\delta\hat{\sigma}_l$. In real space, $E(\underline{r})$ is a matrix of scalar Green functions. The constants A_E and B_E correspond to $\delta(\underline{r})$ terms accounting for core stress changes. The functions $\cos(2n\phi)$ and $\sin(2n\phi)$ are the Fourier transforms of $((-1)^n|n|/\pi r^2)\cos(2n\theta)$ and $((-1)^n|n|/\pi r^2)\sin(2n\theta)$, respectively. The corresponding elements of $E(\underline{r})$ thus decay as $1/r^2$, albeit with various angular dependencies. As an example, a shear stress releasing event $\hat{\underline{\underline{\rho}}}^e = [0, 0, \rho_3]$ with $\rho_3 < 0$, induces a core shear stress drop $B\rho_3\delta(\underline{r}) < 0$, and creates far-field shifts in the three stress components: $\delta\sigma_3 = -(2\gamma_E\rho_3/\pi r^2)\cos(4\theta)$ as found in [30], but also $\delta\sigma_1 = -(\beta_E\rho_3/\pi r^2)\sin(2\theta)$ and $\delta\sigma_2 = (2\gamma_E\rho_3/\pi r^2)\sin(4\theta)$.

A_E and B_E are unknown, because our continuum calculation cannot account for the small scale discreteness [36]. The far-field contributions are set by elasticity: $\alpha_E = (1+\nu)/2$; $\beta_E = 1 - \alpha_E$; $\gamma_E = \alpha_E/2$, with $\nu = \lambda/(2\mu+\lambda)$ the 2D Poisson ratio, and λ, μ the Lamé constants.

In the following, relaxation will be probed using measurements of the correlation matrix of stress *increments*: $C_{ij}(\underline{r}; t) \equiv \langle\delta\sigma_i(\underline{r}_0; t_0, t_0+t)\delta\sigma_j(\underline{r}_0 + \underline{r}; t_0, t_0+t)\rangle$. Within our framework, the stress change accumulated over an arbitrary time interval verifies $\delta\hat{\underline{\underline{\sigma}}}(\underline{k}; t_0, t_0+t) = \hat{E}(\underline{k}) \cdot \hat{\underline{\underline{\rho}}}(\underline{k}; t_0, t_0+t)$, where $\underline{\underline{\rho}}(\underline{r}; t_0, t_0+t) = \sum_e \underline{\underline{\rho}}^e(\underline{r})$ adds up the contributions of all events occurring between t_0 and $t_0 + t$. Thus, in Fourier space: $\hat{C}_{ij} = \langle\delta\hat{\sigma}^*_i\delta\hat{\sigma}_j\rangle = \hat{E}^*_{ik}\hat{E}_{jl}\langle\hat{\rho}^*_k\hat{\rho}_l\rangle$ (with $*$ the complex conjugate) and, since $\hat{E}$ is real,

$$\hat{C} = \hat{E} \cdot \hat{S} \cdot \hat{E}^T, \tag{2}$$

with ^{T} the transpose and $\hat{S} = \langle\hat{\underline{\underline{\rho}}}^*\hat{\underline{\underline{\rho}}}\rangle$ the autocorrelation matrix of the source field.

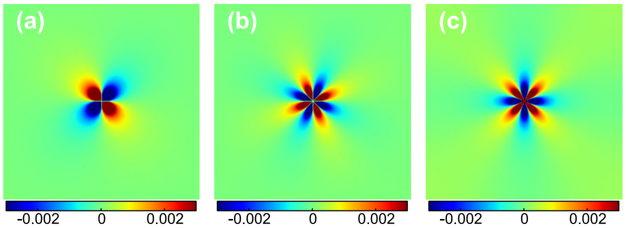

FIG. 3 (color online). For $L = 160$, $T = 0.26$, $t = 100$. 2D plots of (a) $\mathcal{C}_{13}(\underline{r};t)$, (b) $\mathcal{C}_{23}(\underline{r};t)$, and (c) $\mathcal{C}_{33}(\underline{r};t)$.

Typical data for $\mathcal{C}_{13}(\underline{r};t)$, $\mathcal{C}_{23}(\underline{r};t)$, and $\mathcal{C}_{33}(\underline{r};t)$ are presented as 2D plots [Fig. 3] and cuts [Fig. 4(a)], for $T = 0.26$ and $t = 100$. Quite remarkably, they present exactly the r^{-2} scaling forms of the corresponding element of (1) [last column]: $\mathcal{C}_{13} \propto -\sin(2\theta)/r^2$, $\mathcal{C}_{23} \propto \sin(4\theta)/r^2$, and $\mathcal{C}_{33} \propto -\cos(4\theta)/r^2$. To quantify whether $\hat{\mathcal{C}}$ is precisely of the form (1), we define

$$X_n^{ij}(r;t) = -\frac{1}{2\pi^2}\frac{r^2}{r_c^2}\int_0^{2\pi} d\theta \frac{\mathcal{C}_{ij}(\underline{r};t)}{\mathcal{C}_{33}(\underline{0};t)}\cos(n\theta), \qquad (3)$$

and, likewise, Y_n^{ij} with $\sin(n\theta)$ under the integral ($r_c = 1$ is the coarse-graining length). All these quantities are normalized by $\mathcal{C}_{33}(\underline{0};t)$: this choice is of no consequence since $\mathcal{C}_{22}(\underline{0};t) = \mathcal{C}_{33}(\underline{0};t)$ (by isotropy) and, as seen on Fig. 4(b), $\mathcal{C}_{11}(\underline{0};t) \simeq 2\mathcal{C}_{33}(\underline{0};t)$ at all times.

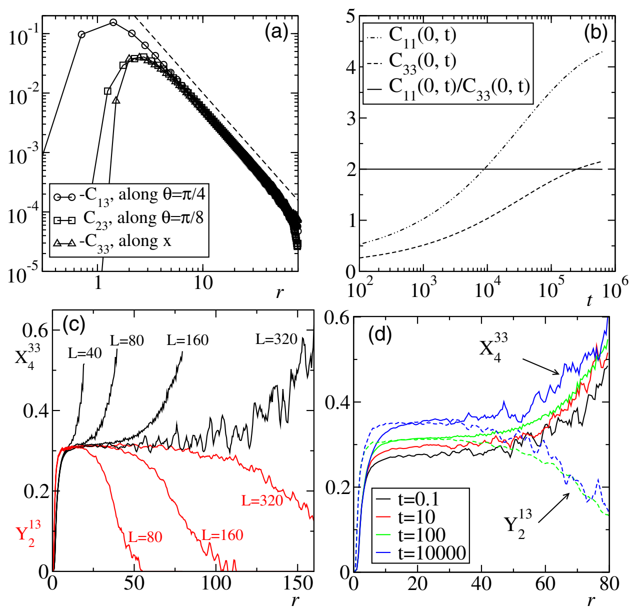

FIG. 4 (color online). Temperature $T = 0.26$. (a) At $t = 100$ cuts of $\mathcal{C}_{13}$, $\mathcal{C}_{22}$, and $\mathcal{C}_{33}$ along appropriate axes; the dashed line has slope -2. (b) $\mathcal{C}_{11}(0,t)$, $\mathcal{C}_{33}(0,t)$, and their ratio vs t. (c) At $t = 100$, $Y_2^{13}(r;t)$ (red) and $X_4^{33}(r;t)$ (black) vs r, for increasing Ls. (d) Y_2^{13} (dashed) and X_4^{33} (full lines) vs r at increasing times up to τ_α.

Y_2^{13} and X_4^{33}, respectively, probe the $-\sin(2\theta)/r^2$ form of $\mathcal{C}_{13}$ and the $-\cos(4\theta)/r^2$ form of $\mathcal{C}_{33}$. They are plotted vs r on Fig. 4(c), for $T = 0.26$, $t = 100$, and increasing Ls. Beyond distances $\simeq L/4$, X_4^{33} rises conspicuously while Y_2^{13} drops. This is a finite size effect, which arises because, in size-L systems, $\mathcal{C}_{ij}$ adds up all periodic image correlations [40]. With increasing L each set of curves develops a plateau; hence, the $\propto 1/r^2$ scalings hold at long range in the $L \to \infty$ limit.

Using X_n^{ij} and Y_n^{ij} we have systematically tested the presence, in every $\mathcal{C}_{ij}(t)$, of all $\cos(n\theta)/r^2$ and $\sin(n\theta)/r^2$ contributions up to $n = 8$ and for t ranging from 0.1 to $10^6 \gg \tau_\alpha$. We thus establish that $\hat{\mathcal{C}}$ presents the terms expected for the Eshelby Green function, and them only: it is of the form (1) with > 0 coefficients at all times.

It is quite remarkable that the stress increment correlation function $\mathcal{C}$ presents the exact scaling form of the Eshelby Green function E. How can it be so?

To interpret this observation, let us denote $\mathbb{M}$ the five-parameter family of matrices of the form (1). The key to the following discussion is that $\mathbb{M}$ is a matrix algebra: it is invariant by addition, multiplication, transpose and by inversion for invertible matrices.

For very short time windows ($t \lesssim 0.1$), less than one event is present in our system, on average: $\hat{\mathcal{S}}$ is thus diagonal and since $\langle\rho_2^2\rangle = \langle\rho_3^2\rangle$ by isotropy, it is an $\mathbb{M}$ matrix. If $\hat{E}$ is an $\mathbb{M}$ matrix, as we anticipate, then by virtue of Eq. (2), $\hat{\mathcal{C}}$ must also present the form (1). Our short time $\mathcal{C}$ data [Fig. 4(d)] are direct evidence that such is indeed the case, and thereby demonstrate that events do create Eshelby fields. Meanwhile they fix A_E and B_E [36].

At finite times, events must correlate, otherwise stress fluctuations would grow unboundedly. Since $\hat{E}$ is known from short time data, the correlations between Eshelby sources can be accessed by deconvolution: $\hat{\mathcal{S}} = \hat{E}^{-1}\cdot\hat{\mathcal{C}}\cdot(\hat{E}^T)^{-1}$. Since both $\hat{E}^{-1}$ and $(\hat{E}^T)^{-1}$ are $\mathbb{M}$ matrices, our observation that $\hat{\mathcal{C}}$ is an $\mathbb{M}$ matrix at all times now proves that $\hat{\mathcal{S}}$ is a product of $\mathbb{M}$ matrices, and, hence, that it is always of the form (1). We thus establish that the correlations between sources are power-law scaling in space with the same radial and angular dependencies as the Eshelby-Green tensor E.

To implement this deconvolution and access the correlations between events, we need to characterize more precisely the time dependence of $\hat{\mathcal{C}}$. Its coefficients are denoted $A_\mathcal{C}$, $B_\mathcal{C}$, $\alpha_\mathcal{C}$, $\beta_\mathcal{C}$ ($=\alpha_\mathcal{C}$ by symmetry), $\gamma_\mathcal{C}$. We saw in Fig. 4(b) that $A_\mathcal{C}(t) \equiv \mathcal{C}_{11}(0,t)$ and $B_\mathcal{C}(t) \equiv \mathcal{C}_{33}(0,t) = \mathcal{C}_{22}(0,t)$ verify $A_\mathcal{C}(t) \simeq 2B_\mathcal{C}(t)$ for all t. We also report, in Fig. 4(d), Y_2^{13} and X_4^{33} data at increasing t: their plateaus grow over the considered time range, and hence the weight of power-law correlations respective to stress fluctuations. Both plateaus, however, collapse at all times: after Fourier transforming, it entails $\gamma_{\mathcal{C}}(t)/\alpha_{\mathcal{C}}(t) \simeq 1/2$. To sum up, we observe, at all times

$$A_{\mathcal{C}}(t)/B_{\mathcal{C}}(t) \simeq 2 \quad \text{and} \quad \gamma_{\mathcal{C}}(t)/\alpha_{\mathcal{C}}(t) \simeq 1/2. \qquad (4)$$

Hence, $\hat{\mathcal{C}}$ explores a two-parameters family of matrices of the form (1), with $A_{\mathcal{C}}(t) \simeq 2B_{\mathcal{C}}(t)$ characterizing stress fluctuations, and $\alpha_{\mathcal{C}}(t) \simeq 2\gamma_{\mathcal{C}}(t)$ the power laws.

The properties (4) introduce two constraints on the coefficients of $\hat{\mathcal{S}}$: $A_{\mathcal{S}}$, $B_{\mathcal{S}}$, $\alpha_{\mathcal{S}}$, $\beta_{\mathcal{S}}$ $(= \alpha_{\mathcal{S}})$, and $\gamma_{\mathcal{S}}$. Using (2) and (4), it appears that the ratios $A_{\mathcal{S}}/B_{\mathcal{S}}$ and $\alpha_{\mathcal{S}}/\gamma_{\mathcal{S}}$ are t independent. Hence, like $\hat{\mathcal{C}}$, the source correlation matrix $\hat{\mathcal{S}}$ explores a two-parameter subset of $\mathbb{M}$, with $A_{\mathcal{S}}$ characterizing the fluctuations of the dipole density and $\alpha_{\mathcal{S}}$ the amplitude of the correlation between events. Moreover, the ratios $\kappa_{\mathcal{C}} \equiv \alpha_{\mathcal{C}}/A_{\mathcal{C}}$ and $\kappa_{\mathcal{S}} \equiv \alpha_{\mathcal{S}}/A_{\mathcal{S}}$ are related by [36]:

$$\kappa_{\mathcal{C}} = \frac{\kappa_{\mathcal{S}} a + b}{\kappa_{\mathcal{S}} c + d} \quad \text{or} \quad \kappa_{\mathcal{S}} = \frac{b - \kappa_{\mathcal{C}} d}{\kappa_{\mathcal{C}} c - a}, \qquad (5)$$

where the constants a, b, c, and d are combinations of the coefficients of $\hat{E}$ [36]. $\kappa_{\mathcal{C}}$ and $\kappa_{\mathcal{S}}$ characterize the relative amplitude of power law correlations in $\hat{\mathcal{C}}$ and $\hat{\mathcal{S}}$. Since all other features of the correlation matrices $\hat{\mathcal{C}}$ and $\hat{\mathcal{S}}$ are set by (4), Eq. (5) and its inverse fully specify the relation between stress increment and source correlations.

Our normalization of (3) was so chosen that $\kappa_{\mathcal{C}} \simeq$ the height of the X_4^{33} plateau, which is reported in Fig. 5 vs t for different T's. $\kappa_{\mathcal{S}}$ is then inferred using (5). It is very clear that the amplitude of power-law correlation grows at early times, peaks, and later recedes. Filled symbols are added at the time $\tau_\alpha(T)$, measured using macroscopic stress relaxation [19,36], to show that it corresponds approximately to the peak time.

Let us now come back to the anisotropies evidenced in the stress field on Fig. 1. At long time, $\mathcal{C}_{ij}(\underline{r}; t \to \infty) = 2\langle \sigma_i(\underline{r}_0 + \underline{r}; t_0)\sigma_j(\underline{r}_0; t_0)\rangle$: this equation results only from stationarity and from the existence of a finite memory time τ_α; hence, it expresses that the equilibrium stress is stationary. To test it, we have systematically analyzed the autocorrelation matrix $\langle \sigma_i \sigma_j \rangle$ of the stress field and found that it indeed presents the very same features as $\mathcal{C}$: not only are σ_2 and σ_3 anisotropic [see Fig. 1] but cross-correlations are present in the IS stress exactly as described in Eq. (1). Moreover, the X_4^{33} plot for $\langle \sigma_i \sigma_j \rangle$ provides $t \to \infty$ values for $\kappa_{\mathcal{C}}$, which are reported near the right edge of Fig. 5 and match quite well its $t = 0$ value. This is expected because $\underline{\underline{\rho}}$ must become spatially uncorrelated at long times, hence $\hat{\mathcal{S}}$ diagonal. The IS local stress is thus statistically equivalent to the stress generated by a space-filling set of spatially and tensorially uncorrelated sources and captures the Eshelby signature.

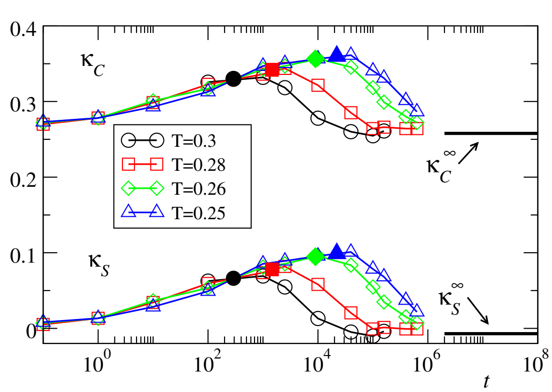

FIG. 5 (color online). For different Ts: $\kappa_{\mathcal{C}}$, the height of the X_4^{33} plateau, and $\kappa_{\mathcal{S}}$ as inferred from [36]; arrows points to the $t \to \infty$ values obtained from $\langle \sigma_i \sigma_j \rangle$ data; filled symbols mark the times $\tau_\alpha(T)$.

How can we explain the initial growth and later decay of power-law correlations? At any arbitrary initial time t_0, and some point $\underline{r}$, the local stress deviates by $\Delta\underline{\underline{\sigma}}(\underline{r}; t_0) = \underline{\underline{\sigma}}(\underline{r}; t_0) - \langle \underline{\underline{\sigma}} \rangle$ from its mean. Relaxation must drive back any initial deviation of the local stress towards the mean, otherwise stress fluctuations would grow unboundedly. This entails that at any point $\underline{r}$, the events that oppose the initial $\Delta\underline{\underline{\sigma}}(\underline{r}; t_0)$ are slightly favored at future times $(t_0 + t > t_0)$. Events thus anticorrelate with the t_0 stress pattern, which is power law correlated. We reason that events thereby acquire power law correlations of growing amplitude at small t; these correlations recede as the memory of the t_0 pattern is gradually erased. This mechanism self-consistently defines a peak time which is $\simeq \tau_\alpha$; it thus appears to control structural relaxation. The peak amplitude, moreover, grows with decreasing T, showing that stress biases play an increasingly important role in the relaxation process near the glass transition.

The picture we propose for supercooled-liquid relaxation is finally that (i) it proceeds via the accumulation of Eshelby events with random core dipole tensors, (ii) the equilibrium IS stress accumulates these fluctuations over times $\gg \tau_\alpha$ and thus presents the same power-law correlations as the Eshelby-Green function, and (iii) the events that eventually erase an initial stress pattern are biased by it and thus transiently develop power-law correlations. There is nothing specific about two dimensions in our argument and we are thus confident that it should carry over to three dimensions.

It is noteworthy that the long-range correlations between relaxation events evidenced here were not captured in studies of so-called "dynamical heterogeneities" [41]. In retrospect, this term appears quite ambiguous: it purports to refer to (a) the relaxation events, but was really used for (b) mobility heterogeneities. The relation between (b) and (a), however, was never clarified, and we now see that mobility-based observables miss long-ranged correlations, and, hence, cannot be considered as characterizing relaxation events. These prior works, moreover, concluded that the relaxation process decorrelates exponentially because all the considered observables did. But if this were true, *all* observables should decorrelate at least exponentially, which is ruled out by the presence of power-law correlations between Eshelby sources. Our observation thus invalidates the existence of a characteristic length scale beyond which the relaxation process decorrelates, and as a corollary, any analogy between the glass transition and critical phenomena.

The author is indebted to Christiane Caroli for her critical readings and insightful comments at key stages of this work.

*anael.lemaitre@ifsttar.fr

[1] M. M. Hurley and P. Harrowell, Phys. Rev. E **52**, 1694 (1995).
[2] R. Yamamoto and A. Onuki, J. Phys. Soc. Jpn. **66**, 2545 (1997).
[3] R. Yamamoto and A. Onuki, Phys. Rev. E **58**, 3515 (1998).
[4] C. Donati, J. Douglas, W. Kob, S. Plimpton, P. Poole, and S. Glotzer, Phys. Rev. Lett. **80**, 2338 (1998).
[5] L. Berthier, Phys. Rev. E **69**, 020201 (2004).
[6] L. Berthier, D. Chandler, and J. P. Garrahan, Europhys. Lett. **69**, 320 (2005).
[7] J. P. Bouchaud and G. Biroli, Phys. Rev. B **72**, 064204 (2005).
[8] A. Cavagna, Phys. Rep. **476**, 51 (2009).
[9] G. Szamel and E. Flenner, Phys. Rev. Lett. **107**, 105505 (2011).
[10] A. S. Keys, L. O. Hedges, J. P. Garrahan, S. C. Glotzer, and D. Chandler, Phys. Rev. X **1**, 021013 (2011).
[11] J. C. Dyre, N. B. Olsen, and T. Christensen, Phys. Rev. B **53**, 2171 (1996).
[12] J. C. Dyre, Phys. Rev. E **59**, 7243 (1999).
[13] J. C. Dyre, T. Christensen, and N. B. Olsen, J. Non-Cryst. Solids **352**, 4635 (2006).
[14] J. C. Dyre, Rev. Mod. Phys. **78**, 953 (2006).
[15] K. Trachenko and V. V. Brazhkin, J. Phys. Condens. Matter **20**, 075103 (2008).
[16] A. Furukawa and H. Tanaka, Phys. Rev. Lett. **103**, 135703 (2009).
[17] A. Widmer-Cooper and P. Harrowell, Phys. Rev. E **80**, 061501 (2009).
[18] K. Trachenko and V. V. Brazhkin, J. Phys. Condens. Matter **21**, 425104 (2009).
[19] A. Furukawa and H. Tanaka, Phys. Rev. E **84**, 061503 (2011).
[20] J. C. Dyre and W. H. Wang, J. Chem. Phys. **136**, 224108 (2012).
[21] S. Abraham and P. Harrowell, J. Chem. Phys. **137**, 014506 (2012).
[22] F. Puosi and D. Leporini, J. Chem. Phys. **136**, 041104 (2012).
[23] V. A. Levashov, J. R. Morris, and T. Egami, J. Chem. Phys. **138**, 044507 (2013).
[24] M. Mosayebi, P. Ilg, A. Widmer-Cooper, and E. Del Gado, Phys. Rev. Lett. **112**, 105503 (2014).
[25] M. Goldstein, J. Chem. Phys. **51**, 3728 (1969).
[26] F. H. Stillinger and T. A. Weber, Science **225**, 983 (1984).
[27] B. Doliwa and A. Heuer, Phys. Rev. E **67**, 030501 (2003).
[28] J. D. Eshelby, Proc. R. Soc. A **241**, 376 (1957).
[29] W. Slaughter, *The Linearized Theory of Elasticity*, 1st ed. (Birkhäuser, Boston, 2001).
[30] G. Picard, A. Ajdari, F. Lequeux, and L. Bocquet, Eur. Phys. J. E **15**, 371 (2004).
[31] C. E. Maloney and A. Lemaître, Phys. Rev. E **74**, 016118 (2006).
[32] A. Lemaître and C. Caroli, Phys. Rev. Lett. **103**, 065501 (2009).
[33] J. Chattoraj, C. Caroli, and A. Lemaître, Phys. Rev. Lett. **105**, 266001 (2010).
[34] J. Chattoraj, C. Caroli, and A. Lemaître, Phys. Rev. E **84**, 011501 (2011).
[35] J. Chattoraj and A. Lemaître, Phys. Rev. Lett. **111**, 066001 (2013).
[36] See Supplemental Material at http://link.aps.org/supplemental/10.1103/PhysRevLett.113.245702 for technical details.
[37] I. Goldhirsch and C. Goldenberg, Eur. Phys. J. E **9**, 245 (2002).
[38] C. Kittel, *Introduction to Solid State Physics* (Wiley, New York, 1995).
[39] F. Leonforte, A. Tanguy, J. P. Wittmer, and J. L. Barrat, Phys. Rev. B **70**, 014203 (2004).
[40] By symmetry, $\mathcal{C}_{13}(\underline{r}) = 0$ on the boundary of the square cell, while $\mathcal{C}_{33}$ is enhanced at $r = L/2$ due to negative lobes overlap.
[41] L. Berthier and G. Biroli, Rev. Mod. Phys. **83**, 587 (2011).